Solid Motor Aft Closure Insulation Erosion

E. Stampfl* and E. M. Landsbaum†
The Aerospace Corporation, El Segundo, Calif.

The erosion rate of aft closure insulation in a number of large solid propellant motors was empirically analyzed by correlating the average ablation rate with a number of variables that had previously been demonstrated to affect heat flux. The main correlating parameter was a heat flux based on the simplified Bartz heat transfer coefficient corrected for two-dimensional effects. A multiplying group contained terms related to port-to-throat ratio, local wall angle, grain geometry, and nozzle cant angle. The resulting equation gave a good correlation and is a useful design tool.

Nomenclature

A,B,C,D = regression coefficients
a,b,c,d = regression coefficients
A_b = asymmetric grain base area, m^2(in.^{2})
A_p = port area, m^2(in.^{2})
C_{DB} = base drag coefficient
C_p = specific heat, cal/gm K (Btu/lb°R)
c^* = characteristic velocity, m/sec(fps)
$\dot{E}$ = energy flux, W/cm^2 (Btu/sec-in.^{2})
H = port-to-throat ratio
K = constants
L = chamber length, m(in.)
M = Mach number
MW = molecular weight, g/mol (lb/mol)
$\dot{m}$ = mass flow, kg/sec (lb/sec)
Q = effective heat of ablation, cal/g (Btu/lb)
P = average chamber pressure, N/cm^2(lb/in.^{2})
$\dot{q}$ = heat flux, w/cm^2(Btu/in.^{2}-sec)
q_p = port dynamic pressure, N/m^2(lb/in.^{2})
R = radius, m(in.)
R' = effective bend radius of curvature, m (in.)
r = radial coordinate, m (in.)
$\dot{r}$ = regression rate, cm/sec (mils/sec)
S = submergence depth, m (in.)
T_o = total temperature, K(°R)
T_w = wall temperature, K(°R)
t = exposure time, sec
V_b = gas radial velocity at propellant surface, m/sec (fps)
V_r = radial velocity component, m/sec (fps)
V_z = axial velocity component, m/sec (fps)
V_∞ = freestream velocity, m/sec (fps)
W = power, W/cm^2(ft-lb/sec-in.^{2})
X = effective cavity length, m(in.)
α = cant angle, radians
β = fraction of impinging particles
γ = specific heat ratio
ϵ = emissivity
ρ = density, kg/m^3(lb/in.^{3})
θ = wall angle, deg
σ = Stefan-Boltzmann const., W/K^{4}m^2(Btu/sec-in.^{2}-R^4)
ϕ = average entrance angle, deg

Subscripts

B = simplified Bartz
BP = simplified Bartz evaluated in port
BS = simplified Bartz corrected for sink flow
c = convection
p = port
r = radiation, radial
s = submerged
t = throat
z = axial

Presented as Paper 73-1238 at the AIAA/SAE 9th Propulsion Conference, Las Vegas, Nevada, November 5-7, 1973; submitted November 25, 1974; revision received April 22, 1975. This work was performed under Air Force Contract F04701-73-C-0074 and NASA Contract NASw-2301.

Index categories: Solid and Hybrid Rocket Engines; Material Ablation.

*MTS, Propulsion Department. Member AIAA.
†Section Manager, Propulsion Department. Member AIAA.

I. Introduction

PREDICTIONS of solid motor aft closure insulation erosion rates have, in general, not been satisfactory. The most recent example was the burn-through on the first firing of the 120-in. 7 segment motor although it had been designed with a safety factor of 2 based on the Titan III-120 in. 5 segment results.[1] In several instances, erosion rates have been significantly underpredicted, which resulted in marginal conditions, although, not resulting in catastrophic motor failure. In other cases, the erosion rates were significantly overpredicted, resulting in unnecessary overdesigns.

The sophistication of the insultion design analysis techniques employed vary, ranging from simple regression rate correlations with area ratio, to elaborate potential flow, particle impingement, reacting boundary-layer analysis. The increased sophistication in analysis does not, in general, correspond to improved regression rate prediction. Similar conclusions have been reached for heat flux measurements in liquid engine models.

The lack of agreement between theoretical and actual insulation performance and analysis limitations suggest a semi-empirical approach for the prediction of insulation performance. The analysis presented here is based on perturbing the simplified heat flux by terms showing the influence of port-to-throat ratio, wall angle, noncircular ports, and nozzle cant angle. The approach is novel in that the perturbation terms are derived from fluid dynamic considerations and experiments such as flow over asymmetric steps and curved ducts. The resulting good correlation has a lower variability than the normal equation using simple heat transfer only and will be very useful in the design of large solid rocket motors such as those for the Space Transportation System (STS). One should note that the correlation does not include any data on submerged canted nozzles although the problem is discussed.

II. Erosion Rate Problems

The inadequacy of current insultation regression rate prediction techniques for large motors was most recently demonstrated on the Titan IIIM program. Prior to the design of the seven segment motor, five segment motor aft closure

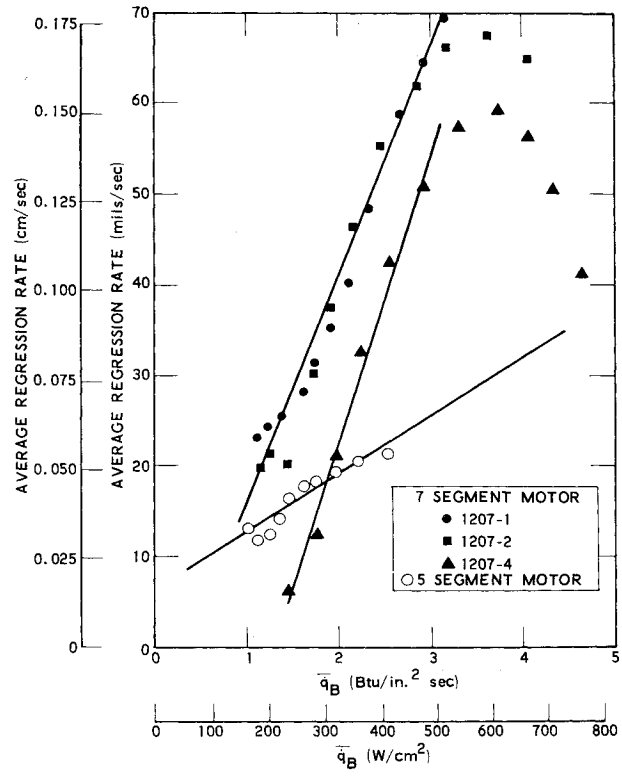

Fig. 1 Titan III five- and seven-segment motors aft-closure insulation erosion.

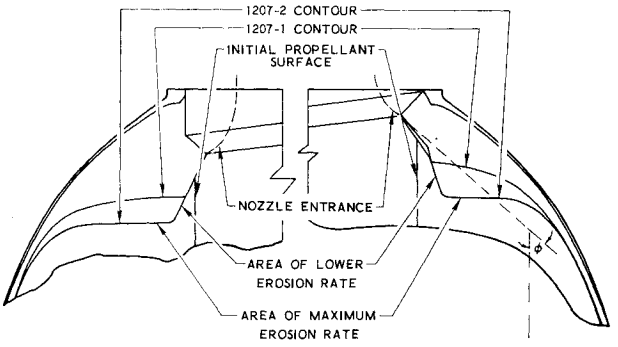

Fig. 2 Seven-segment aft closure.

rubber (V-44) regression rates were correlated with simplified Bartz heat flux. The linear correlation of several firings was good as indicated by the data given in Fig. 1. The 7 segment motor aft closure insulation (ORCO 9250) was designed assuming the same correlation to hold after it was demonstrated by subscale testing that the two rubbers were equivalent. The V-44 and ORCO 9250, both silica-asbestos loaded BUNA-N rubbers, had also previously been shown to be equivalent when a material change was incorporated in the Titan IIIC Motor. The success of the substitution of ORCO 9250 for V-44 on Titan IIIC has been demonstrated by several subscale tests and successful flights.

The design of the 7 segment motor aft closure insulation based on the indicated approach was not successful. The first motor experienced an aft closure burn-through although a safety factor of 2 was incorporated.[1] The inadequacy of the design approach is clearly shown by the comparison of the 7 segment motor regression rates and those of the 5 segment motor of Fig. 1. The regression rates of the first 7 segment motor firing at the same Bartz heat flux level were by about a factor 2.5 greater than those of the 5 segment motor.

The aft closure insulation thickness was increased for the subsequent 1207 motors.[2] This was accomplished by displacing the 1207-1 aft closure contour forward, and thereby maintaining a similar contour except for the aft most region where the convergence half-angle is low (Fig. 2). The regression rates of the third firing, the data of which is not shown in the figure, was similar to that of the first 2 firings. The regression rates of the fourth firing were lower, and the decreasing trend in the aft most region more pronounced than that of the previous firings but still within the expected random variations. The reduction in erosion rate in the high heat flux region occurred in a region of lower wall angles (Fig. 2). The aft closure design change resulted in successful tests, except that it apparently adversely affected the performance of the nozzle lead ring.

A recent re-evaluation of the 5 and 7 segment motor data,[3] using more sophisticated analytical tools (which included two-dimensional potential flow solutions, boundary-layer, and particle impingement analyses), resulted in no significant improvement in understanding the test results. The results did indicate that such an approach could be successful but that the present analytical tools are insufficient. Improvements are required in particle size prediction, impingement analysis, and asymmetric subsonic flow analysis.

Historically, the first significant large solid motor insulation performance prediction discrepancy occurred on the 100-in. diam FW-2.[4] In this case, the predicted rubber regression rate was by about a factor of 1.5 higher than that observed. The predicted FW-2 regression rates at the various area ratios were obtained from similar data obtained on the 100-in. FW-1 corrected for mass flux. The discrepancy was initially blamed on the under-cured state of the insulation in the FW-1.

Although the current aft closure insulation performance analysis is limited to large solid motors, the experience of 2 smaller motors, the Castor II[5,6] and Zeus,[7] is pertinent. The aft closure erosion rate difference between Castor II-3 and Castor II-5 is attributable to the effect of nozzle cant. The 2 motors are identical except for the 11° cant of the II-5 motors. The average aft closure insulation regression rate of II-5 motors is about 50% greater than that of the II-3 motors. Full-scale motor experience and cold flow tests conducted for Zeus Stage II[7] show the effect of aft end grain geometry on nozzle wall heat flux. The data show that the effect of grain star points can increase the local heat flux by several hundred percent above that given by developed flow correlations.

III. Development of Regression Rate Correlation

The principal reasons for the lack of agreement between theory and experiment appear to have been: 1) inadequately defined freestream flow and its effect on boundary layer; 2) inadequately defined entrance boundary layer and particle conditions; and 3) undefined relationship between particle impact and material removal. Although adequate capability exists to determine boundary-layer development and particle impingement for a given freestream flowfield, the overall results are not adequate due to uncertainties concerning the freestream flow. For typical solid motor designs, the state-of-the-art freestream flow analysis capability is limited to idealized two-dimensional potential flow solutions. Particle agglomeration analysis capability, aside from uncertainties about the initial size distribution, is also limited. For most solid motor designs, these freestream flow analysis limitations are so significant that detailed boundary layer and particle trajectory analysis may not be warranted, since both require a freestream flow definition. These limitations suggest a less detailed but more inclusive approach to insulation regression rate prediction.

The evaluation of various apparently uncorrelated rocket nozzle heat transfer and regression rate data has, through theoretical considerations and the hypothesis of mechanisms, led to the definition of 5 dominant regression rate correlation parameters. The following development is given to show the rationale for the choice of these parameters rather than their theoretical justification.

Regression rate data of solid motor insulation materials are typically available as exposure time averaged values. It is, therefore, natural to attempt a correlation using exposure time-averaged independent parameters. To simplify the effort, circumferentially averaged rates and parameters will be correlated. The local variations as they occur in asymmetric designs will be treated separately. Based on steady-state energy considerations, the exposure time average rubber regression rate within the expected accuracy of the overall approach is given by

$$\bar{\dot{r}} = (1/t) \int_o^t \dot{r}\, dt = (\bar{\dot{E}}/\rho Q) \tag{1}$$

where the symbols are defined in the nomenclature. The energy flux includes thermal as well as mechanical energy and work done on the surface by a two-phase freestream. The total energy flux to the surface is the sum of the convective and radiative flux, the flux of thermal energy due to particle impingement, and the mechanical energy input to the surface,

$$\bar{\dot{E}} = \bar{\dot{q}}_c + \bar{\dot{q}}_r + \bar{\dot{q}}_p + \bar{\dot{W}} \tag{2}$$

To define the total energy flux, the various components will be treated separately.

The convective heat flux component is taken as the simplified Bartz heat flux[8] modified for specific conditions which are not accounted for by the Bartz correlation, but have been found to affect aft closure and nozzle heat flux. The simplified Bartz heat flux was chosen since it is simple, and since it correlates experimental results in idealized nozzle entrance regions about as well as more sophisticated approaches.[9]

The modification to be included consists of 4 perturbations to the Bartz heat transfer coefficient in terms of port-to-throat ratio, contraction angle, aft end grain geometry, and nozzle cant angle. Aside from the perturbations noted, the Bartz heat flux was adjusted to account for two-dimensional mass flux effects. Since the aft end motor designs of interest incorporate average contraction half-angles between about 40° and 75°, it was considered necessary to correct the local one-dimensional mass flux used in the Bartz correlation. This was accomplished by correcting the one-dimensional area used in the Bartz heat flux to the area of the corresponding spherical zone. The correction which assumes the flow on the average to be a spherical sink flow with half-angle ϕ (Fig. 2) is appropriate since any consistent deviation from sink flow as exists in the throat and entrance regions is adequately accounted for by a proportionality constant. The convection perturbations to the Bartz heat flux are included, similar to the inclusion of perturbations due to entrance length, curvature, proturberance, etc., to developed flow heat flux.

Port-to-Throat Ratio Effect

The normalized perturbation of the local heat flux in the convergent section due to changes in the port-to-throat ratio was taken to be proportional to $\bar{H}$ based on the data of Refs. 10 and 11 which show an approximate linear relationship to exist. From a physical point of view, the port-to-throat ratio accounts for boundary-layer starting conditions and boundary-layer development, through its effect on the freestream velocity and total pressure distribution. In solid motors, the effect is particularly large since the port mass addition significantly alters the entrance velocity distribution. According to Culick,[12] the axial velocity distribution at the aft end of a solid motor is given by

$$V_z = V_b \pi\ (L/R_p) \cos\ (\pi r^2/2R_p^2) \tag{3}$$

Culick's theoretical results are in good agreement with the experimental results of Ref. 13. Equation (3) shows that the axial velocity distribution is a direct function of the motor length to radius ratio (L/R_p) and the surface blowing velocity, which in turn is directly related to propellant burning rate. For typically large solid motor grain designs, this is in turn directly related to the port-to-throat ratio through continuity requirements. The perturbation in heat flux due to boundary-layer starting and developing conditions as they are affected by the incoming velocity and total pressure distributions, should therefore, correlate with the exposure time average port-to-throat ratio, $\bar{H}$.

Local Wall Angle Effect

The heat flux perturbation due to change in the contraction angle was taken to be proportional to sin θ. The data of Ref. 10 indicates that in the region of practical entrance angles this is not unreasonable. From a physical point of view, the contraction angle affects boundary-layer starting condition and development. The local contraction angle effect, although treated in this way, is probably not independent of port-to-throat ratio. A treatment in terms of configuration integrals as proposed by Ref. 14 may, therefore, be more appropriate.

Grain Geometry Effect

The perturbation of the Bartz heat flux due to variations in the aft end grain geometry was taken to be proportional to the ratio of the rate of work done by the base drag of the asymmetric grain base area divided by the freestream energy flow. Because of the abrupt change in flow cross-sectional area at the downstream grain termination, the flow separates and induces secondary flow in the grain base region. The heat flux in typical symmetric separated regions such as downstream facing steps, except for the reattachment region, is low due to the low local velocities. The heat flux in asymmetric separated regions, however, such as in the base regions of proturberances and star grains, can be several times that of the corresponding freestream, due to high secondary velocities and disrupted boundary layer.[7] As a result, the asymmetric portion of the base area rather than the total base area is considered pertinent. The asymmetric base area is the solid area within the circle just encompassing the port area. The rate of work done by the corresponding base drag is a measure of energy dissipation or heat flux, the freestream energy flow rate being a convenient reference variable. The base drag power is given as

$$\text{Drag Power} = C_{DB} A_b\ q_p\ V_z \tag{4}$$

and the total port energy flow rate is given as

$$\text{Energy Flow} = \rho A_p\ C_p T_o V_z \tag{5}$$

If one neglects the relatively small Reynolds number influence on the drag coefficient, the port kinetic energy flow rate, and limits the application to subsonic flow, the heat flux enhancement due to grain geometry is approximately given by

$$\overline{(A_b/A_p)\ M_p^2} \tag{6}$$

Nozzle Cant Effect

The perturbation of the convective heat flux due to nozzle cant should correlate similar to bend loss coefficients.[15] The principal difference between bend correlations and canted nozzle solid motor correlation attempted here, is the deletion of the Reynolds number and inclusion of motor L/R. Solid motor port velocity profiles exhibit shapes that are between laminar and turbulent profiles. The rationale for the substitution is that secondary flow in bends is the result of lateral velocity gradients as shown by Ref. 16 and that in solid motors the port exit velocity profile strongly depends on $\dot{r}L/R$. To maintain the heat flux perturbation term nondimensional, this is approximated as L/R. This is not unreasonable, considering that burning rate variations of in-

terest are relatively small. The curvature effect is retained as $(R/R')^{1/2}$ as given by Ref. 17. The canted nozzle perturbation heat flux for a cant angle α is then proportional to

$$\overline{(L/R_p)\ (R/R')^{1/2}\alpha} \tag{7}$$

Radiation, Particles, Mechanical Effects

The radiation heat flux, although numerically not negligible, has been shown to contribute little to rubber regression in regions of low convective heat flux, perhaps due to formation of char. In regions of high convective heat flux or wall shear, radiation damage may be significant. Since the radiation flux is similar for all motors considered, and since it is partly correlatied through the convective flux terms, the radiation heat flux component is not explicitly included.

The heat flux due to particle impingement is given by the excess heat content transferred to the surface by impinging particles. Based on theoretical considerations, the fraction of impinging particles is dependent on the motor port-to-throat ratio as it affects particle momentum, on contraction angle, aft end grain geometry, and nozzle cant as these affect particle turning. Within the accuracy of the current approach, the fraction of impinging particles, and consequently the particle heat flux was considered given by an expression analogous to that for the convective heat flux. Since all motors had propellants with approximately the same aluminum content (15-20%), separating out particle effects would be difficult.

By limiting the correlation to noncharring ablators and by neglecting the difference between local static and wall temperature as well as neglecting the particle kinetic energy, one can argue that mechanical energy input to the surface need not be explicitly included. Mechanical energy input under these conditions is given by terms analogous to those for convection.

Final Regression Equation

The final insulation regression rate correlation equation applicable to the aft end regions of conventional motor designs is

$$\dot{r}=A\dot{q}_B\left[\frac{1+\cos\phi}{2}\right]^{0.9} \times (1+a\bar{H}+b\sin\theta + c\ \overline{(A_b/A_p)M_p^2} + d\ \overline{(L/R_p)\ (R/R')^{1/2}\alpha}\ ) \tag{8}$$

IV. Available Data

The compilation of aft end insulation data was limited to large solid motors and several small motors that exhibited design features similar to large motors. The parameters of those motors included in the current evaluation are given in Table 1, and all regression rate parameters for each motor are presented in Table 2. The correlation was also limited to equivalent rubber insulations. ORCO 9250 and V-44 have been shown to be equivalent.[18] It was not known whether TI-0700A, a Thiokol material used in the Castor II motors was equivalent to V-44, the more commonly used material, and as a result was treated in a separate correlation. The current results, however, show that separate treatment is not necessary.

FW-1

The reported regression rates[4,19] were assumed to be circumferentially averaged values. The average contraction half-angle used to correct the one-dimensional mass flux was obtained graphically as an effective entrance angle. The local angle corresponds to that of the prefire contour. The accuracy of both the average and local contraction angles, since they were obtained from small sketches,[19] may not be as good as one would like. The accuracy uncertainty also applies to the exposure time averaged port-to-throat ratio, since accurate grain design details were not available. The same problem applies to the grain base area. Although these variables were not precisely established, the accuracy is adequate for the proposed correlation.

FW-2

The uncertainty about the average regression rate[4] and average port area does not apply since the motor had a circular port grain. The question regarding the accuracy of the contraction angles still exists, since they were obtained from a small sketch.

SS-120 and SL-260

The reported regression rate data[20,21] at various circumferential locations was arithmetically averaged. The

Table 1 Motor parameters

Motor	R_t (in.)	R' (in.)	L (in.)	H	MW (lb/lb mol)	γ	T_o (°R)	C_p (Btu/lb-°R)	c* (ft/sec)	ϕ (deg)
FW-1	12.9			3.327	27	1.18	6080	0.45	5060	58
FW-2	14.2			1.817	27	1.18	6360	0.44	5120	55
SS-120	15.15			2.14	26.2	1.17	6090	0.45	5170	64
SL-260	35.5			3.28	26.2	1.17	6090	0.45	5170	48
L-71	18.68			7.45	24.8	1.19	5847	0.45	5200	56
L-72	18.62			2.98	25.0	1.19	5880	0.45	5190	56
TU-412	19.0			3.1	28.45	1.18	6240	0.46	5173	50
CASTOR II-3	4.15			1.69	27.8	1.17	6525	0.42	5227	40
CASTOR II-5	4.15	24.0	200	1.69	27.8	1.17	6525	0.42	5227	40
1205	18.85	80	796	2.13	25	1.18	6160	0.44	5100	75
1207-1	20.8	120	1038	1.74	25	1.18	6160	0.44	5100	55
1207-2	20.8	120	1038	1.74	25	1.18	6160	0.44	5100	50
1207-4	20.8	120	1038	1.74	25	1.18	6160	0.44	5100	50
SUBSCALE SEVEN SEG.	3.15			1.74	25	1.18	6160	0.44	5100	65

question of accuracy regarding contraction half-angles, exposure time average port-to-throat ratio, and propellant grain base area applies to both motors, since design drawings were not available. As before, the accuracy is considered adequate for the proposed correlation.

L-71 and L-72

For the 156-in. diam L-71 and L-72 motors,[22,23] the accuracy in contraction half-angle is better than that of the 260-in. program motors. Both motors had circular port grains and as a result, the exposure time average port-to-throat was readily established.

TU-412

The comments about the accuracy of the contraction angle made for the 156-in. LPC motors[24] apply to the 156-in. TU-412 motor as well. An additional uncertainty concerning the cant angle exists for this motor since the nozzle was gimbaled. In the gimbal duty cycle the average gimbal angle is small and as a result was not included in the correlation.

Castor Motors

The insulation material[5,6] is a Thiokol product TI-0700A loaded with carbon and glass which at low Mach numbers (less than 0.05) is equivalent to V-44.[25] The contraction angle uncertainty discussed earlier on other motors does not apply in this case as design drawings were available from which the angles were obtained.

Titan III

The regression rates,[3] except for the subcale motor, are circumferential averaged values computed from 8 measurements. The given averages correspond to locations at a constant initial radius from the motor center line. The contraction angle uncertainty discussed earlier does not apply since the angles were taken from half-scale design layouts. The motor length was used for L, the radius of the aft closure port was used for R_p.

V. Correlation Results and Applicability

A linear regression correlation corresponding to Eq. (8) was performed to establish 5 correlation constants. The actual correlation calculations were carried out with Eq. (8) multiplied out to make use of existing automated regression analysis capability. Although the rearrangement introduces some uncertainties regarding the regression coefficients, they are well within the overall accuracy.

The following correlation was obtained by using the data of all motors (except the two Castor II motors)

$$\bar{r}=A\bar{q}_B(1+\cos\phi/2)^{0.9}\times[1-0.12\bar{H}+4.0\sin\theta$$
$$+472\overline{(A_b/A_p)M_p^2}+1.48\overline{(L/R_p)(R/R')^{1/2}\alpha}] \quad (9)$$

where $A=5.34\times10^{-5}$ cm$^3/J$(3.44 mils in.^{2}/Btu). The correlation coefficient corresponding to the previous relation is 88% and the residual standard deviation is 0.021 cm/sec (8.2 mils/sec). The standard deviation of the heat of ablation constant (A) is 6.51×10^{-5} cm$^3/J$ (4.2 mils in.^{2}/Btu). Estimates of the regression constants indicate that all correlation parameters are significant at a level of about 5%.

The correlation for the Castor II data, if one assumes the correlation constants of the perturbation energy terms to be independent of the material, give $A=4.3\times10^{-5}$ cm$^3/J$ (2.8 mils in.^{2}/Btu). The correlation is good with a residual standard deviation of 0.012 cm/sec (4.6 mils/sec). Since the heat of ablation constant for the latter data is satistically no different from that of Eq. (13), it is reasonable to assume that both sets of data from a regression point of view are part of the same population. The limited data of Ref. 25 indicate that this is not unreasonable. The correlation using all data gives the following results

$$\bar{r}=A\bar{q}_B[1+\cos\phi/2]^{0.9}$$
$$\times[1-0.091\bar{H}+1.77\sin\theta+235\overline{(A_b/A_p)M_p^2}$$
$$+0.63\overline{(L/R_p)(R/R')^{1/2}\alpha}] \quad (10)$$

The correlation coefficient is 91% with a residual standard deviation of 0.019 cm/sec (7.5 mils/sec). The standard deviation of the heat of ablation constant (A) is 4.97×10^{-5} cm$^3/J$ (3.2 mils in.^{2}/Btu). All regression constants are significant at a level of about 5%. A comparison of computed and measured regression rates is shown in Fig. 3.

Several other correlations were attempted, including log linear, but with no significant improvement in correlation. Changes in the correlation variables included the Bartz heat flux without the two-dimensional correction, use of the maximum intial port Mach number multiplied by the propellant aluminum content instead of the time averaged port-to-threat ratio, and the use of the average rather than local contraction half angle. None of the attempted correlations resulted in a better correlation.

To assess the improvement of the correlation achieved by Eq. (10) over that of a simple correlation with Bartz heat flux, the available data was correlated against Bartz heat flux with the following results

$$\bar{r}=-0.011\text{ cm/sec }(4.4\text{ mils/sec})+23.8$$
$$\times10^{-5}\text{cm}^3/J\ (15.3\text{ mils in.}^2/\text{Btu})\,\bar{q}_B \quad (11)$$

The corresponding correlation coefficient is 59% with a residual standard deviation of 0.030 cm/sec (12 mils/sec). The improved correlation achieved by Eq. (10) is significant.

The regression rate relation given by Eq. (10) can, due to the physical significance of the correlation parameters, be confidently applied to new designs for which the parameters are within the range of the data used to establish the relation. The exposure time average port-to-throat ratio range is 4.5-16.0, the contraction angle range is from near zero to 75°, the wall angle from 0-90°, the range in the aft end grain geometry parameter is 0-0.0067, and the cant angle range is from 0-11°. The minimum area ratio for which data was available is 1.42.

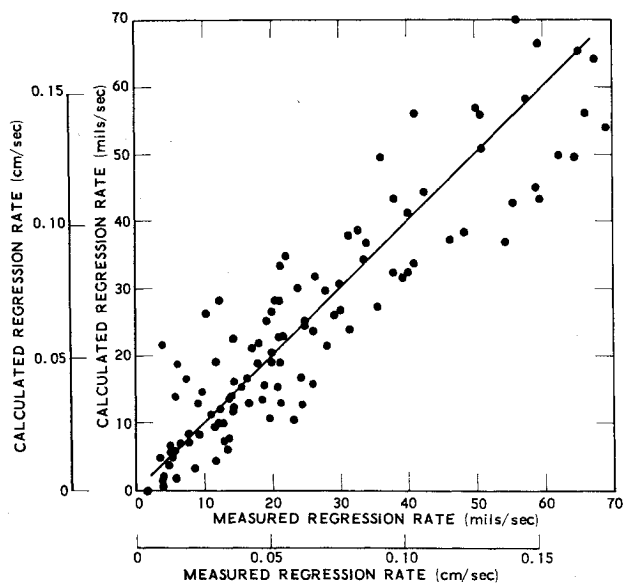

Fig. 3 Correlation results.

Table 2 Regression rate parameters

Motor	R in.	$\bar{\dot{r}}$ mils/sec	$\bar{P}$ lb/in^2	$\overline{\dot{q}_{BS}}$ Btu/in^2-sec	$\bar{H}$	sin θ	$\overline{(A_b/A_p)M_p^2}$	$\frac{L}{R_p}\left(\frac{R}{R'}\right)^{1/2}\alpha$ radians	References
FW-1	39.5	5	566	0.864	11.95	0.616	0.0007		4,19
	31.4	24	541	1.260	9.87	0.809	0.0018		
	26.7	30	541	1.686	8.76	0.883	0.0039		
	23.6	36	541	2.105	8.06	0.914	0.0067		
FW-2	43.4	5	432	0.740	10.78	0.629			4
	34.5	9	514	1.28	8.810	0.727			
	29.3	17	547	1.81	7.75	0.814			
	25.9	28	562	2.31	7.10	0.868			
	23.55	34	570	2.77	6.66	0.888			
	21.8	38	574	3.20	6.35	0.893			
SS-120	25	40.1	517	2.11	7.78	0.766	0.0052		20,21
	27.5	33.5	538	1.84	8.24	0.891	0.0040		
	30	10.2	541	1.58	8.72	0.950	0.0025		
	32.5	3.8	551	1.39	9.22	0.995	0.0016		
SL-260	85.5	5.7	533	1.06	9.13	0.906	0.0007		20,21
	62.5	39.3	533	1.86	7.28	0.906	0.0024		
	59.0	54.4	533	2.06	7.01	0.906	0.0029		
	55.8	59.3	533	2.28	6.78	0.766	0.0045		
L-71	71.4	3.9	513	0.474	15.9	0.530			22,23
	63.6	11.6	541	0.609	14.3	0.766			
	54.6	13.4	555	0.817	12.6	0.829			
	44.2	16.5	548	1.18	12.2	0.895			
	36.0	19.9	548	1.71	12.2	0.906			
	34.3	21.0	548	1.86	12.2	0.917			
	29.8	23.7	548	2.40	12.2	0.903			
	29.2	24.8	548	2.49	12.2	0.676			
L-72	63.6	5.3	602	0.669	14.3	0.766			22,23
	54.6	9.4	624	0.904	12.6	0.839			
	44.2	9.6	634	1.34	10.6	0.888			
	34.3	24.7	617	2.06	10.2	0.921			
	29.2	25.9	616	2.76	10.2	0.574			
TU-412	72	3.75	543	0.502	15.4	0.316			24
	68	3.75	579	0.585	14.6	0.488			
	63	4.60	611	0.701	13.6	0.574			
	57	6.50	648	0.880	12.4	0.731			
	50	10.8	686	1.17	11.2	0.799			
	46.5	13.7	696	1.34	10.6	0.819			
	43.4	18.8	697	1.52	10.0	0.804			
	41.0	20.8	694	1.68	9.64	0.695			
CASTOR II-3	8.29	21.9	638	2.83	8.01	0.876			5,6
	9.11	21.4	655	2.44	8.58	0.838			
	9.91	21.6	673	2.14	9.15	0.795			
	10.63	21.0	688	1.92	9.69	0.748			
	11.45	15.4	697	1.72	10.2	0.697			
	12.0	14.4	703	1.57	10.7	0.642			
	12.6	12.6	703	1.44	11.2	0.584			
	13.1	13.7	698	1.33	11.7	0.522			
	13.7	13.2	688	1.22	12.1	0.457			
	14.0	11.6	688	1.17	12.4	0.390			
	14.4	8.5	688	1.11	12.7	0.321			
	14.7	5.8	688	1.08	12.9	0.250			
	14.9	3.7	688	1.05	13.2	0.177			
	15.0	1.6	688	1.03	13.2	0.104			
CASTOR II-5	9.91	31.2	673	2.14	9.15	0.795		1.64	5,6
	10.6	26.3	688	1.92	9.69	0.748		1.59	
	11.4	19.9	697	1.72	10.2	0.697		1.55	
	12.0	14.1	703	1.57	10.7	0.642		1.52	
CASTOR II-5	12.6	11.7	703	1.44	11.2	0.584		1.49	5,6
	13.1	14.4	690	1.33	11.7	0.522		1.46	
	13.7	18.5	688	1.22	12.1	0.457		1.43	
	14.0	14.1	688	1.17	12.4	0.390		1.42	
	14.4	12.0	688	1.11	12.7	0.321		1.40	
	14.7	7.6	688	1.08	12.9	0.250		1.39	
	14.9	7.6	688	1.05	13.2	0.177		1.38	
	15.0	5.4	688	1.03	13.2	0.104		1.37	
	15.1	3.3	688	1.02	13.3	0.030		1.37	
1205	53.7	13.0	447	0.668	9.09	0.438		1.03	3
	51.2	11.7	453	0.736	8.70	0.574		1.05	
	48.2	12.3	461	0.832	8.24	0.676		1.08	
	46.5	14.1	466	0.895	7.98	0.755		1.10	
	44.6	16.4	472	0.974	7.70	0.848		1.12	
	42.7	17.9	478	1.06	7.42	0.897		1.14	
	40.7	18.0	485	1.17	7.13	0.937		1.16	
	38.7	19.2	493	1.30	6.85	0.966		1.18	
	36.6	20.5	502	1.46	6.57	0.952		1.21	
	34.3	21.2	513	1.67	6.26	0.977		1.24	

Table 2 Regression rate parameters (continued)

Motor	R in.	$\bar{\dot{r}}$ mils/sec	$\bar{P}$ lb/in^2	$\overline{\dot{q}_{BS}}$ Btu/in^2-sec	$\bar{H}$	sin θ	$\overline{(A_b/A_p)M_p^2}$	$\overline{\frac{L}{R_p}\left(\frac{R}{R'}\right)^{1/2}}^{\alpha}$ radians	References
1207-1	55.3	23.1	451	0.922	7.68	0.350		1.08	3
	53.3	24.4	458	0.997	7.42	0.485		1.11	
	50.6	25.9	469	1.12	7.07	0.581		1.14	
	47.2	28.1	483	1.30	6.64	0.734		1.17	
	45.4	31.4	491	1.41	6.42	0.757		1.19	
	43.4	35.2	499	1.55	6.18	0.788		1.22	
	41.5	40.0	508	1.70	5.95	0.891		1.24	
	39.5	48.2	517	1.88	5.72	0.976		1.26	
	37.0	59.0	530	2.16	5.44	0.989		1.30	
	35.5	64.5	537	2.35	5.27	0.990		1.32	
	34.2	69.3	544	2.54	5.13	0.990		1.33	
1207-2	55.2	19.8	463	0.982	7.67	0.334		1.09	3
	53.3	21.2	470	1.06	7.42	0.448		1.11	
	50.1	20.0	482	1.21	7.01	0.701		1.14	
	46.0	30.1	499	1.45	6.49	0.891		1.19	
	43.7	37.7	508	1.61	6.21	0.993		1.21	
	41.2	46.3	519	1.82	5.92	0.999		1.24	
	38.7	55.3	531	2.08	5.63	0.989		1.27	
	36.1	62.0	543	2.39	5.34	0.978		1.31	
	34.2	66.0	552	2.67	5.13	0.970		1.33	
	32.1	67.4	560	3.03	4.90	0.962		1.36	
	30.3	65.0	566	3.39	4.71	0.786		1.39	
1207-4	50.8	6.07	503	1.22	7.09	0.682		1.13	3
	46.0	12.4	523	1.50	6.49	0.905		1.19	
	43.7	21.1	533	1.67	6.22	0.991		1.21	
	41.2	32.6	544	1.89	5.92	0.998		1.24	
	38.8	42.4	556	2.14	5.64	0.991		1.27	
	36.4	51.0	568	2.45	5.37	0.974		1.30	
	34.2	57.4	578	2.77	5.13	0.966		1.33	
	32.1	59.3	587	3.15	4.90	0.961		1.36	
	30.7	56.2	592	3.43	4.75	0.883		1.39	
	29.8	50.6	595	3.63	4.66	0.454		1.40	
	28.7	41.1	598	3.90	4.55	0.358		1.42	
SUBSCALE	5.87	7.43	458	1.32	7.27	0.857			3
SEVEN	5.13	17.2	497	1.59	6.85	0.902			
SEGMENT	4.44	29.2	528	1.89	6.46	0.908			
	3.50	40.8	540	2.38	5.87	0.917			

The applicability of Eq. (10) to aft closure designs for which the heat flux perturbation parameters are outside the range investigated requires further considerations. From an overall point of view, the high correlation coefficient, which is a measure of the linear dependence of regression rate on the independent parameters, indicates that a linear extrapolation beyond the range of the actual data is justifiable.

By concentrating on the individual perturbation terms, additional confidence in applying the correlation beyond the range of the correlation parameters is obtained. The linear dependence of heat flux on port-to-throat ratio over a range from 1.0-19.0[11] indicates the linear relationship of Eq. (10) to be applicable in the low port-to-throat ratio region. The linear dependence of the velocity profile, particle agglomeration and mean port velocity in the low subsonic region on port-to-throat ratio further indicates a linear relationship to be adequate.

A wall angle extrapolation for conventional designs is not expected to be necessary since the correlation data includes angles of up to 90°. The linear relationship indicated by Eq. (10) is appropriate considering that particle slip is a linear function of the sine of the turning angle. The regression rate correlation to submerged nozzle designs is not directly applicable. Aft closure regression rate predictions of submerged nozzle designs will be discussed later.

The heat flux perturbation due to aft end grain geometry variations is based on energy dissipation due to base drag. A linear relationship between heat flux and base drag work rate in the subsonic flow regime is justified through Reynolds analogy. As a result, the correlation can be extrapolated to all practical aft end grain designs.

The heat flux perturbation, due to nozzle cant, is correlated with the total head loss coefficient of bends except that L/R_c was substituted for the Reynolds number function. Bend loss coefficient data for bend angles of 45, 90, and 180° correlate linearly with bend angle. Linear extrapolation of the correlation given by Eq. (10) to practical nozzle cant angles is, therefore, expected to be reasonable.

Aside from the possible errors introduced by not explicitly including particle damage, mechanical work done on the surface, and radiation, the accuracy of the given correlation also suffers since interaction terms were not included. By eliminating these shortcomings of the current approach, it is believed that the empirical approach of solid motor insultation design techniques can be further improved. A reasonable improvement goal would be to reduce the residual standard deviation to about 0.01 cm/sec (4 mils/sec), which is a typical estimate of random variability.

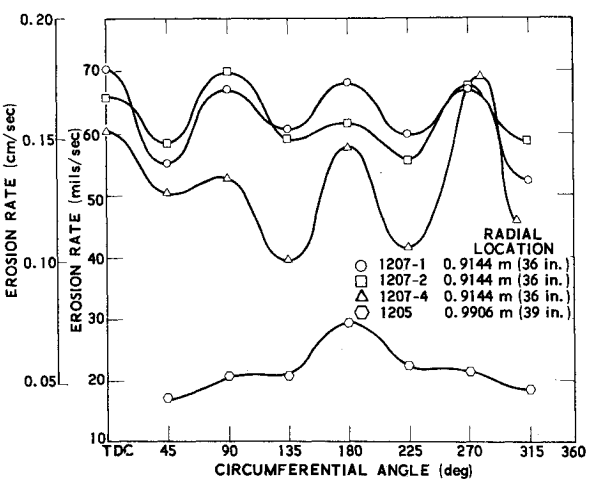

Fig. 4 Circumferential aft-closure erosion rate.

VI. Circumferential Variation

The correlation given by Eq. (10) is expected to provide a reasonable prediction of the exposure time and circumferential averaged regression rate at specific axial locations in the aft closure. For asymmetric designs with either asymmetric grain configurations or canted nozzles, the circumferential variation in regression rate must be accounted for. The local regression rate in line with star valleys or the regression rate at the outside of the bend (BDC) of canted nozzle configurations can be significantly higher than the circumferential averaged regression rate.

The regression rate data which is part of the current evaluations (Table 1) is not adequate to establish a correlation for the circumferential regression rate variation. Since canted nozzles are of interest, the circumferential variation of regression rate due to cant warrants some comments. The circumferential variation in regression rate experienced on the Titan III SRM's are shown in Fig. 4. From the data given in the figure, it was concluded that the aft closure rubber regression rate in the pitch and yaw planes is significantly higher than in the 45° planes, and that the nonuniform regression rate exists in the 5- as well as 7-segment motors. The regression rate at BDC is not significantly higher than at the inside of the bend (TDC) as one would expect. The regression rate patterns resemble the convective heat flux patters in bends.[26,29] The observed pattern can be physically related to locations of maximum velocity and particle impingement (BDC) minimum shedding layer thickness (90 and 270°) and disrupted boundary layer (TDC). The circumferential regression rate variation in the aft closure of Castor II-5 motors has not been conclusively established because of a lack of data. The circumferential rate variation in the nozzle entrance region of the Castor II-5 motors, however, is very evident as the erosion at BDC is about 50% greater than that at TDC. The circumferential variation in regression rate is probably most readily estimated in terms of the local average rate. The Titan III and the Castor II data show that the maximum circumferential deviation in regression rate aside from random variations is about 15% higher than the average. Additional data, however, should be evaluated to establish a design tool to account for circumferential regression rate variations in canted nozzle motor designs.

VII. Effects of Nozzle Submergence

A design concept of interest is a submerged nozzle. The correlation given by Eq. (10) is not applicable, but a few words are in order. A submerged symmetrical nozzle design, where the submergence is greater than R_t in a symmetrical motor, presents no aft closure problems as shown by Refs. 28 and 29. The aft closure regression rates are low corresponding to nearly forward closure rates. The regression rates may be correlated with the heat flux values observed in cavities, and an application of this approach is given in Ref. 30. The heat flux is expected to vary with the port-to-throat ratio as indicated by the dependence of heat flux on upstream flow.

In the case of an asymmetric design such as a canted submerged nozzle, the average regression rates are expected to be higher than those of symmetrical design as a result of an enhancement in heat flux due to secondary flow. The local regression rates are expected to vary circumferentially similar to those of a conventional canted nozzle design. Although much additional work is needed to enable the prediction of regression rates for this design, an approximate assessment is possible using the previously indicated approach and the data of Ref. 31. The average aft closure regression rate for a symmetric, submerged nozzle design using heat flux correlation techniques is

$$\bar{\dot{r}}_p = A\bar{\dot{q}}_{BP}\ \overline{(X/S)^{0.3}} \qquad (12)$$

where the constant $A = 3.1 \times 10^{-5}$ cm^3/J(2.0 mils in.^{2}/Btu) was based on fitting the data of Ref. 31 and the exponent from the data of Ref. 32. The heat flux $\dot{q}_{BP}$ corresponds to the average Bartz aft port heat flux, X is the average difference of the port radius minus the nozzle entrance radius, and S is the nozzle submergence depth. Equation (12) is expected to apply when X/S is between about 0.25 and 1.75. To account for the average regression rate enhancement due to cant, the perturbations developed for conventional nozzle design are expected to give best estimate results. The circumferential variation is also expected to be similar to conventional nozzle designs.

The treatment of local regression rates and the treatment of submerged nozzles is based on very limited data, additional work is obviously required before a satisfactory design tool is established. the procedure indicated should, however, give a reasonable estimate of aft insulation performance for submerged canted nozzle designs.

VIII. Summary

A correlation of aft closure insultation erosion rates of a number of large solid rocket motors has resulted in a usable engineering design equation. The correlation equation presented is a considerable improvement over the normal equation using only heat flux. It shows the importance of port-to-throat ratio, entrance angle, local wall angle, grain design, length-to-radius ratio, and cant angle. Even more important it appears that motor designs where the equation would indicate high erosion rates or where the equation might not be applicable can be tested in scale motors. The erosion rate in aft closures with submerged nozzles is low and comparable to that in forward closures. The major area neglected is the possible effect of particles due either to differences in amount or size or to effects resulting from flowfields materially different from those in the motors used in the correlation. However, such effects could be obtained in scale motor tests. The techniques used in the paper could be used to analyze similar problems such as erosion in blast tubes, heat transfer in liquid engines, which are not easily amenable to a purely theoretical approach.

References

[1] "Titan III/M 1207-1 Detailed Static Test Evaluation Report," Rept. 4802-69-145, and Addendum, June 1969, United Technology Center, Sunnyvale, Calif.

[2] "Static Test Evaluation Report 1207-2," Rept. 4404-70-58, April 1970, United Technology Center, Sunnyvale, Calif.

[3] "Titan III Seven Segment Analytical Study Final Report," Rept. 4310-72-36, March 1972, United Technology Center, Sunnyvale, Calif.

[4] "Preliminary 100 FW-1 Motor Firing Report," Rept. 06292, Aug. 1961, Aerojet General Corp., El Monte, Calif.

[5] "Test Report TX 354-3 Rocket Motors 6, 7, 5 and 22 Preliminary Flight Rating Test Castor II Program," Rept. C-65-7029A, Sept. 1965, Thiokol Chemical Corp., Bristol, Pa.

[6] "Test Report TX 354-5 Rocket Motor Demonstration Program," Rept. C-67-1004A, April 1967, Thiokol Chemical Corp.

[7] Bremberg, N. A. and Stampfl, E., "Wind Tunnel Study of Surface Flows and Heat Flux in Nike Zeus Sustainer Propellant and Grain Base Region," Paper 3719, July 1966, Douglas Aircraft Co., Long Beach, Calif.

[8] Bartz, D. R., "A Simple Equation for Rapid Estimation of Rocket Nozzle Convective Heat Transfer Coefficients," *ARS Journal*, Vol. 27, Jan. 1957, pp. 49-51.

[9] Parkins, R. C., "Convective Heat Transfer in Rocket Engine," Rept. 67/11, Oct. 1967, Rocket Propulsion Establishment Technical Rept., Westcott, England.

[10] Von Glahn, U. H., "Correlation of Gas Side Heat Transfer for Axisymmetric Rocket Engine Nozzles," TM X-1748, Feb. 1969, NASA.

[11] Boldman, D. R., Schmidt, J., and Gallagher, A., "Laminarization of a Turbulent Boundary Layer as Observed from Heat Transfer and Boundary Layer Measurements in Conical Nozzles," TN D-4788, Sept. 1968, NASA.

[12]Culick, F. E. C., "Rotational Axisymmetric Mean Flow and Damping of Acoustic Waves in a Solid Propellant Rocket," *AIAA Journal,* Vol. 4, Aug. 1966., pp. 1462-1465.

[13]Hermsen, R., private communications, June 1972, United Technology Center, Sunnyvale, Calif.

[14]Mayer, E., "Analysis of Convective Heat Transfer in Rocket Nozzles," presented at 15th ARS Annual Meeting, Washington, D. C., Dec. 1960.

[15]Ito, H., "Friction Factors for Turbulent Flow in Curved Pipes," *Journal of Basic Engineering,* June 1959, pp. 131-143.

[16]Hawthorne, W. R., "Secondary Circulation in Fluid Flow," *Proceedings of the Royal Society London,* Vol. 206, 1951, pp. 374-387.

[17]Schlichting, H., *Boundary Layer Theory,* McGraw-Hill, New York.

[18]"Subscale Test Evaluation Report for Titan III/M," Rept. 4802-66-123, Dec. 1966, United Technology Center, Sunnyvale, Calif.

[19]"100 FW-2 Motor Firing Report," April 1962, Aerojet General Corp., April 1962, El Monte, Calif.

[20]"Static Test Firing of Motor 120-SS-1," CR-54864, Jan. 1965, NASA.

[21]"260 Inch Diameter Motor Feasibility Demonstration Program," CR-54865, Oct. 1965, NASA.

[22]"156 Inch Diameter Motor Jet Tab TVC Program," AFRPL-TR-64-167, Vol. I, Jan. 1965, Air Force Rocket Propulsion Lab., Edwards Air Force Base, Calif.

[23]"156 Inch Diameter Motor Jet Tab TVC Program," AFRPL-TR-64-167, Vol. IV, Jan. 1965, Air Force Rocket Propulsion Lab., Edwards Air Force Base, Calif.

[24]"156 Inch Diameter Motor Movable Nozzle Program," AFRPL-TR-65-4, Aug. 1965, Air Force Rocket Propulaion Lab., Edwards Air Force Base, Calif.

[25]"Critical Design Review TX 526 Castor IV Rocket Motor," C-69-02, Jan. 1969, Thiokol Chemical Corp., Bristol, Pa.

[26]Harvey, D. and McRae, R., "Flow Studies in Propulsion System Ducting," Paper 2085, Douglas Aircraft Co., April 1964, Long Beach, Calif.

[27]Seban, R. A., "Heat Transfer in Tube Coils with Laminar and Turbulent Flow," *International Journal of Heat Mass Transfer,* Vol. 5, May 1963, pp. 387-395.

[28]"Continuation of Aerodynamic Studies of Immersed-Nozzle Design Parameters for Second State Minuteman Wing. VI, Development," Rept. TM-160, Aug. 1963, Aerojet General Corp., El Monte Calif.

[29]"Determination of Flow Properties in the Aft Chamber Region of the Poseidon C-3 First Stage Motor," TWR-1705, Feb. 1966, Thiokol Chemical Corp., Bristol, Pa.

[30]Hong, Y. S., "Heat Transfer Analysis of the Thiokol TE-M-364-3 Motor," Rept. TOR-0059 (6154-03)-1, March 1971, Aerospace Corp., El Segundo, Calif.

[31]"156 Inch Diameter Motor Liquid Injection TVC Program," AFRPL-TR-66-109, July 1966, Air Force Rocket Propulsion Lab., Edwards Air Force Base, Calif.

[32]Fox, J., "Heat Transfer and Air Flow in a Transverse Rectangular Notch," *International Journal of Heat Mass Transfer,"* Vol. 8, Feb. 1965, pp. 269-279.